PAPER • OPEN ACCESS

Spin-dipole oscillation and relaxation of coherently coupled Bose–Einstein condensates

To cite this article: A Sartori *et al* 2015 *New J. Phys.* **17** 093036

New Journal of Physics
The open access journal at the forefront of physics

Deutsche Physikalische Gesellschaft DPG
IOP Institute of Physics

Published in partnership with: Deutsche Physikalische Gesellschaft and the Institute of Physics

OPEN ACCESS

RECEIVED
15 July 2015

ACCEPTED FOR PUBLICATION
19 August 2015

PUBLISHED
21 September 2015

PAPER

Spin-dipole oscillation and relaxation of coherently coupled Bose–Einstein condensates

A Sartori[1], J Marino[2], S Stringari[1] and A Recati[1,3]

[1] INO-CNR BEC Center and Dipartimento di Fisica, Università di Trento, 38123 Povo, Italy
[2] Institute of Theoretical Physics, TU Dresden, D-01062 Dresden, Germany
[3] Technische Universität München, James-Franck-Strasse 1, 85748 Garching, Germany

E-mail: recati@science.unitn.it

Keywords: coherently coupled Bose–Einstein condensate, paramagnetic—ferromagnetic transition, collective modes, spin-dipole dynamics, spinor order parameter, BECs, Hopf bifurcation

Supplementary material for this article is available online

Abstract

We study the static and the dynamic response of coherently coupled two component Bose–Einstein condensates due to a spin-dipole perturbation. The static dipole susceptibility is determined and is shown to be a key quantity to identify the second order ferromagnetic transition occurring at large inter-species interaction. The dynamics, which is obtained by quenching the spin-dipole perturbation, is very much affected by the system being paramagnetic or ferromagnetic and by the correlation between the motional and the internal degrees of freedom. In the paramagnetic phase the gas exhibits well defined out-of-phase dipole oscillations, whose frequency can be related to the susceptibility of the system using a sum rule approach. In particular in the interaction $SU(2)$ symmetric case, i.e., all the two-body interactions are the same, the external dipole oscillation coincides with the internal Rabi flipping frequency. In the ferromagnetic case, where linear response theory in not applicable, the system shows highly non-linear dynamics. In particular we observe phenomena related to ground state selection: the gas, initially trapped in a domain wall configuration, reaches a final state corresponding to the magnetic ground state plus small density ripples. Interestingly, the time during which the gas is unable to escape from its initial configuration is found to be proportional to the square root of the wall surface tension.

1. Introduction

Ultra-cold gases allow the realizations of multi-component Bose–Einstein condensates (BECs). The latter are novel systems, whose behaviour is very different with respect to that of a single component BEC. In particular they show different zero-temperature phases, each described by a proper vector order parameter. The possibility of tuning a number of system parameters, in particular the interaction strength through Feshbach resonances, makes such systems ideal for studying the structure of the various phases and the nature of the phase transitions.

One of the easiest, but still intriguing realizations is represented by a two-component BEC, also known as a spinor condensate. Spinor condensates allow us to address many interesting phenomena from the Andreev–Bashkin effect [1, 2] and fast decay of persistent currents [3], to the (internal) Josephson effect [4, 5], or Schrödinger-cat- and twin-Fock-like states [6, 7], from dimerized vortices [8–10], to the study of quenching in classical bifurcations [11–13]. They represent also the basis for most of the recent realizations of artificial gauges in cold gases[14] .

In this paper we specifically consider a zero-temperature trapped two-component BEC with an external field that drives the population transfer (spin-flipping) between the two atomic levels (see section 2) forming the condensate. It is common to refer to the interconversion term as a Rabi coupling. The system is indeed a generalization to non-linear atom optics of the well-known linear Rabi problem and in general is an extension of quantum optics concepts to condensates [15, 16]. It is the interplay between the intra- and inter-species two-

body interaction strengths and the Rabi coupling strength that makes the physics of the system very rich. The Rabi coupling—which acts as a σ_x operators on each atom—tries to create an equal superposition of the two possible internal levels. However, differences in the three possible atom–atom interaction strengths try to favour a situation where the population of the two internal levels is unbalanced. It turns out that the system exhibits a second order phase transition, a classical bifurcation at the mean-field level (see, e.g., [17, 18] and in particular the experiment [5]), which is analogous to the mean-field ferromagnetic transition of the Ising model in transverse field. Moreover, if the two components feel different external potentials the internal and external degrees of freedom are inseparable leading to interesting spin–orbit coupled dynamics as has already been shown some years ago in [19, 20].

In the following we show that the static and the dynamic response to an out-of-phase (spin) dipole perturbation is very rich and captures many relevant phenomena related to the paramagnetic/ferromagnetic-like phase transition of the system. A relative component perturbation is accessible in cold gases by applying different trapping potentials for different atomic internal levels. The spin-dipole configuration is realized by applying trapping potentials that have the same shape, but that are displaced for the two components of the gas. The dynamics is obtained by monitoring the gas after the displacement is suddenly set to zero. Notice that in [19, 20] a similar situation has already been realized, but instead the external potentials were held fixed and the Rabi coupling was suddenly turned on.

The main results of our analysis can be summarized as follows:

(i) In the region before the bifurcation occurs, i.e., in the paramagnetic phase, the system exhibits well-defined out-of-phases oscillations around the equilibrium position in the new trapping potential. The oscillation frequency is in good agreement with a sum-rule approach calculation. The latter allows us to identify the main quantity determining the spin-dipole mode frequency and its relation with the susceptibility of the system. In the case of equal interaction strength, the sum rule gives an exact result. The latter is practically twice the Rabi coupling, i.e., the main contribution is not proportional, contrary to the usual case, to the harmonic trapping frequency. This effect can be traced back in the modification of the *f*-sum rule, which is eventually due to the absence of relative number conservation.

(ii) In the broken $\mathbb{Z}_2$, i.e., ferromagnetic phase, the situation is very different. The response of the system to the spin-dipole perturbation is not linear and therefore the initial state in the displaced potentials is far from the equilibrium state when the potentials are the same. In particular the initial configuration shows a polarization domain wall at the centre of the cloud, but zero global polarization, while in the new equilibrium state it will show a symmetric structure with a global polarization. The dynamics is highly non-linear. After a certain period—in which the system is trapped in the domain wall configuration—the cloud is able to reach the new equilibrium quickly by spontaneously selecting one of the two possible polarizations. The excess energy of the initial configuration gives rise to small ripples in the cloud.

It is worth mentioning here that the very same mean-field description we use in the following (see section 2) can be applied, in certain regimes, to describe polariton systems where the role of the polarization is relevant (see e.g., [21, 22]), as well as some properties of type-1.5 superconductors (see [23] and reference therein).

The paper is organized as follows: In section 2 we introduce the system and its description in terms of two coupled Gross–Pitaevskii (GP) equations. We revisit the emergence of a paramagnetic/ferromagnetic-like transition and the effect of the external harmonic trapping potential. In section 3 we study the effect of a spin-dependent potential and the role of the spin-dipole susceptibility. The latter is shown to bear a clear signature of the phase transition. Then we address the problem of the dynamics of the spin-dipole mode, both in the para- and in the ferromagnetic phase. In the former case (section 4.1) linear response theory combined with a sum-rule approach provides an accurate estimate of the spin-dipole mode frequency, which compares well with the numerical solution of the GP equation. In the ferromagnetic case (section 4.2) we show that the system exhibits ground state selection, after a waiting time in which the system is unable to leave the initial domain wall configuration. We found phenomenologically that this characteristic time is proportional to the square root of the domain wall energy.

2. Gross–Pitaevskii equation for coherently coupled BECs

We consider an atomic Bose gas at zero temperature, where each atom of mass m has two internal levels $|a\rangle$ and $|b\rangle$. The latter are typically magnetically trappable hyperfine levels of ^{87}Rb, like $|a\rangle = |F = 1,\ m_F = -1\rangle$ ($|F = 1,\ m_F = 1\rangle$) and $|b\rangle = |F = 2,\ m_F = 1\rangle$ ($|F = 2,\ m_F = -1\rangle$). An external field is applied that coupled the $|a\rangle$ to the $|b\rangle$ state via usually a two-photon transition, characterized by a Rabi splitting Ω. At the densities of ultra-cold gases the atomic interactions are simply described by a contact potential with a strength proportional

to the s-wave scattering length. For a spinor system three scattering lengths, a_{aa}, a_{bb} and a_{ab} are present describing the intra- and the inter-species collisions, respectively. Finally, the condensed phase for a two-component Bose gas is described by a complex spinor order parameter $(\psi_a(\mathbf{r},\, t),\, \psi_b(\mathbf{r},\, t))$, where ψ_i, $i \in \{a,\, b\}$ is the wave function macroscopically occupied by atoms in the internal state $|i\rangle$. The latter is normalized to the total number of atoms N_i in the state $|i\rangle$. The dynamics of the order parameter is determined by coupled Gross–Pitaevskii equations [15, 24]

$$\begin{aligned} \mathrm{i}\hbar\frac{\partial}{\partial t}\psi_a &= \left[-\frac{\hbar^2\nabla^2}{2m} + V_a + g_a\left|\psi_a\right|^2 + g_{ab}\left|\psi_b\right|^2\right]\psi_a + \Omega\psi_b, \\ \mathrm{i}\hbar\frac{\partial}{\partial t}\psi_b &= \left[-\frac{\hbar^2\nabla^2}{2m} + V_b + g_b\left|\psi_b\right|^2 + g_{ab}\left|\psi_a\right|^2\right]\psi_b + \Omega^*\psi_a, \end{aligned} \tag{1}$$

where the couplings g_i, with $i \in \{a,\, b,\, ab\}$, are the intra- and interspecies atomic interaction strengths and are given by $g_i \propto a_i$ [24], and V_a and V_b are the external trapping potentials. We consider the confinement to be harmonic, which is the most relevant and typical experimental situation. In the following, if not differently specified, we consider $g_a = g_b \equiv g$. Due to the presence of the Rabi coupling, only the total number of atoms $N = N_a + N_b$ is conserved, but not its polarization $P = (N_a - N_b)/N$. The (gauge) symmetry of the system is therefore reduced from $U(1) \times U(1)$ to $U(1) \times \mathbb{Z}_2$, leading from an homogeneous condensate to a gapless density or in-phase mode—Goldstone mode of the broken $U(1)$ symmetry—and a gapped spin or out-of phase mode (see, e.g., [17, 18]). Depending on the interaction strengths and the Rabi coupling, the ground state can also spontaneously breaks the $\mathbb{Z}_2$ symmetry leading to $P \neq 0$.

In order to describe the ground state, we write as usual the condensate wave function as density and phase $\psi_i = \sqrt{n_i}\, e^{i\phi_i}$ and use local density approximation (LDA), i.e., neglecting the gradient term, also known as quantum pressure, in equations (1). The time derivative on the lhs of equation (1) is replaced by the chemical potential μ, whose value will be fixed by requiring a total number of particle N. Notice that in the absence of Ω one can have two different chemical potentials reflecting that also P is fixed. The Rabi coupling originates a term of the form $\Omega\cos(\phi_a - \phi_b)$ for the energy. Without any loss of generality we also assumed Ω to be real and positive, which fixes the phases in the ground state to satisfy $\phi_- = \phi_a - \phi_b = \pi$. Finally one finds that the densities of the two components obey the relations (see, e.g. the review [25] and reference therein)

$$\left(g - g_{ab} + \frac{\Omega}{\sqrt{n_a n_b}}\right)\left(n_a - n_b\right) = V_b - V_a, \tag{2}$$

$$\left(g + g_{ab} - \frac{\Omega}{\sqrt{n_a n_b}}\right)\left(n_a + n_b\right) = 2\mu - \left(V_b + V_a\right). \tag{3}$$

For the sake of simplicity and clarity, we consider a mean-field one-dimensional situation. The latter is experimentally realized by making two of the trapping frequencies strong enough for the motion along such directions to be frozen. The coupling constants are in this case renormalized and can be simply related to the scattering length and the trapping transverse frequency $\omega_\perp$ by $g_i = 2\hbar\omega_\perp a_i$ for $i \in \{a,\, b,\, ab\}$. It is worth noticing that our results do not qualitatively change in the two- or three-dimensional case.

From equation (3) it is clear that, for equal potentials, $V_a = V_b$, the system can sustain a finite polarization only if g_{ab} is sufficiently large. In that case it turns out that the $P \neq 0$ states are the ground states of the system. Notice that both the critical value of g_{ab} and P are density dependent. It is easy to find that the points X_P at which the polarized phase can exist is fixed by the condition

$$g_{ab} > g + 2\Omega/n\left(X_P\right) \tag{4}$$

with $n(x) = n_a(x) + n_b(x)$ the total local density. Since in the harmonic trap the density decreases going outward from the trap centre the system can exhibit two different regions: unpolarized tails with $n_a = n_b$ and a polarized core with $n_a \neq n_b$. Clearly, if the condition equation (4) is not satisfied at the centre of the trap, where the total density is maximum, then the whole system is unpolarized. This allows us to introduce a critical value of Rabi coupling defined by

$$\Omega_{\mathrm{cr}} = \frac{1}{2}n(x=0)\left(g_{ab} - g\right) \tag{5}$$

For values $\Omega \geqslant \Omega_{\mathrm{cr}}$ the system is unpolarized everywhere. Writing $V_a = V_b = m\omega_{\mathrm{ho}}^2 x^2/2$, the density profile $n_a = n_b$ is easily obtained from equation (3):

$$n_{a,b}(x) \equiv n_0(x) = \frac{\mu + \Omega}{g + g_{ab}}\left(1 - \frac{x^2}{R_{\mathrm{TF}}^2}\right), \tag{6}$$

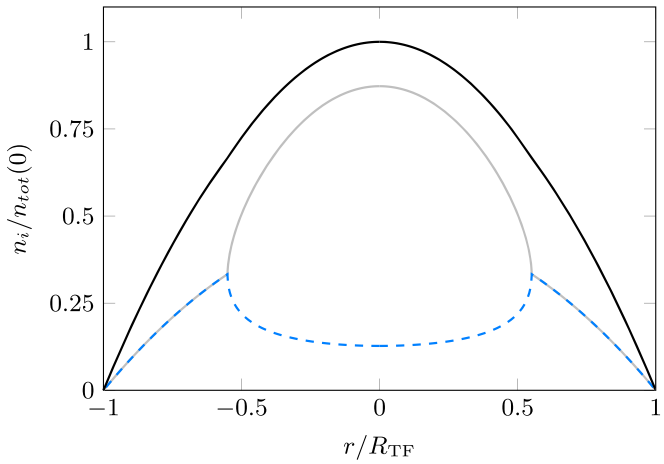

Figure 1. Density profiles within Thomas–Fermi approximation for an harmonic trapping: n_a (dashed blue), n_b (light grey) and $n_a + n_b$ (black) for $g_{ab}/g = 1.3$ and $\Omega/\mu = 0.1$.

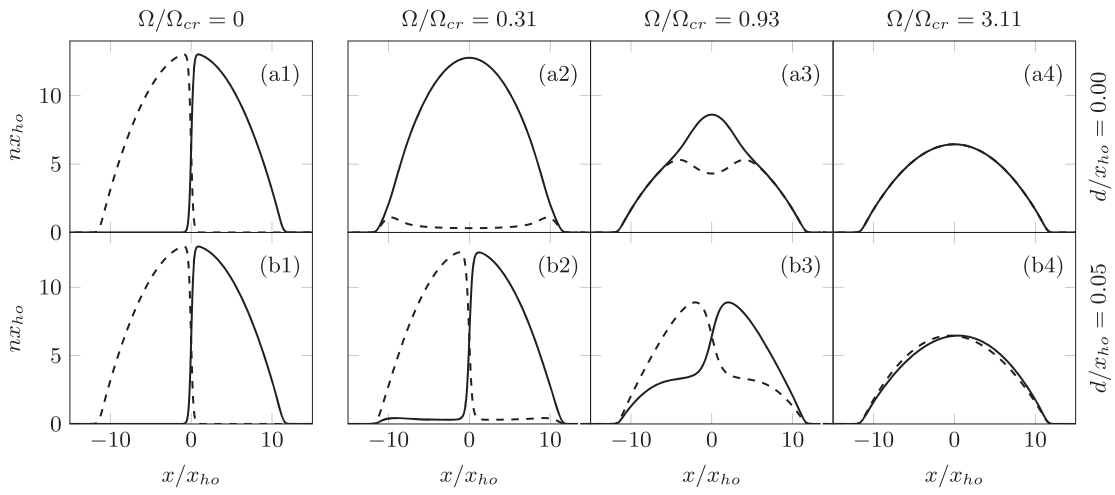

Figure 2. Ground states of a trapped coherently-coupled Bose gas for different values of potential displacement d and Rabi coupling Ω. We use coupling constant strength $g_{ab}/g = 1.1$ and $g/(\hbar\omega_{\rm ho}x_{\rm ho}) = 5$. Plots (a1)–(a4) correspond to $d/x_{\rm ho} = 0$, while plots (b1)–(b4) to $d/x_{\rm ho} = 0.05$. For the ground state in panels 2, 3, and 4 we use the values $\Omega/\Omega_{\rm cr} = 0.31, 0.93, 3.11$, respectively. For comparison we report also the ground state for a Bose–Bose mixture, i.e., $\Omega = 0$. In the latter case, with the number of particles in each component fixed, no global polarization appears, and the ground states (a1) and (b1) are essentially equal. The effect of quantum pressure can be clearly noticed in the plots (a2) and (a3) (analogues to figure 1). The bifurcation points are not sharp as instead predicted by the Thomas–Fermi approximation.

where we introduced the so-called Thomas–Fermi radius $R_{\rm TF}^2 = 2(\mu + \Omega)/(m\omega_{\rm ho}{}^2)$ [24] and the chemical potential can be written as

$$\mu = \left[\frac{3}{8}N\left(g + g_{ab}\right)\right]^{2/3}\left(\frac{m\omega_{\rm ho}}{2}\right)^{1/3} - \Omega. \tag{7}$$

In the case $\Omega < \Omega_{\rm cr}$ a typical configuration within LDA is shown in figure 1.

Let us hgive a brief reminder here that for a Bose–Bose mixture in the absence of Rabi coupling ($\Omega = 0$), where the relative particle number can be chosen at will, the situation is very different. In that case there exists a first order phase transition to a phase separated state once $g_{ab} > g$ and the system in the trap is formed by two distinct regions of only one of the two components of the gas (see for a detailed discussion, e.g. [26–28]). An example of the structure for an equal number of atoms in both hyperfine levels is shown in figure 2(a1).

3. Static dipole polarizability

In this section we calculate the static response of a trapped spinor gas to a spin-dipole perturbation. A spin-dipole perturbation corresponds to a shift of the harmonic traps for the two components by a quantity $d \ll x_{\rm ho}$ with $x_{\rm ho} = \sqrt{\hbar/(m\omega_{\rm ho})}$,

$$\begin{aligned} V_{a,b} &= \frac{1}{2} m {\omega_{\rm ho}}^2 (x \pm d)^2 \\ &= \frac{1}{2} m \omega_{\rm ho}^2 x^2 \pm m \omega_{\rm ho}^2 x d + {\rm O}\left(d^2\right), \end{aligned} \tag{8}$$

where the plus sign is for particles of component a and the minus one for those of component b. In the case of hyperfine atomic levels the displacement can be realized by adding a magnetic field gradient to the harmonic potential.

The GP ground state solution for the spinor gas in the displaced potentials is reported in figure 2 (see also [15]), where for the sake of concreteness we assume $g_{ab} > g$ to show the difference between a mixture and a coherently driven spinor gas. For $d = 0$ (row a) we see the features of the Ω-induced phase transition: below the critical value the linear coupling prevents the phase separation by creating a global polarization in the system (figure 2 plots (a2) and (a3)), while a mixture without any Rabi coupling $\Omega = 0$ would be in a phase separated state (figure 2 plots (a1)). Above the critical value the gas is unpolarized (figure 2 plot (a4)). Applying a potential displacement (row b) makes the local polarization different from zero as shown in equation (2). In this case even a small potential difference makes the ferromagnetic part of the gas strongly polarized and as a result a magnetic domain wall is created at the centre of the trap.

In order to calculate the spin-dipole susceptibility we first determine the spin-dipole moment D, defined as

$$D = \frac{1}{N} \int x \left[n_a(x) - n_b(x) \right] {\rm d}x. \tag{9}$$

The spin-dipole susceptibility is then defined by the limit

$$\chi_{\rm sd} = \lim_{d \to 0} D/\lambda \tag{10}$$

where $\lambda = dm\omega_{\rm ho}^2$ is the perturbation associated with the spin-dependent component of the potential (8).

In the *global paramagnetic phase* ($\Omega > \Omega_{\rm cr}$) it is easy to obtain an analytical expression for $\chi_{\rm sd}$ within LDA. In this case one can employ the energy functional

$$E = \int \left[\chi_s^{-1} \left(n_a - n_b \right)^2 - \lambda x \left(n_a - n_b \right) \right] {\rm d}x \tag{11}$$

relative to the spin degrees of freedom of the problem, where

$$\chi_{\rm s} = \frac{2}{g - g_{ab} + \Omega/n_0} \tag{12}$$

is the spin (magnetic) susceptibility for an homogeneous system of density $2{\rm n}_0$ (see, e.g., [25]). Variation with respect to the spin density $(n_a - n_b)$ yields the result

$$n_a(x) - n_b(x) = x \lambda \chi_{\rm s} \left(n_0(x) \right), \tag{13}$$

and the spin-dipole polarizability finally reads

$$\chi_{\rm sd} = \frac{1}{N} \int x^2 \chi_{\rm s} \left(n_0(x) \right). \tag{14}$$

After integratiion we obtain the result

$$\frac{D}{d} = \frac{g + g_{ab}}{g - g_{ab}} \left[1 + f\left(\frac{\Omega}{\left(g - g_{ab} \right) n_0} \right) \right], \tag{15}$$

for the dimensionless ratio $D/d = m\omega_{\rm ho}^2 \chi_{\rm sd}$ where we have introduced the dimensional function $f(\alpha) = 3\alpha(1 - \sqrt{1+\alpha}\,{\rm arccoth}(\sqrt{1+\alpha}))$ [4] and used the notation $n_0 = n_0(0)$.

A couple of comments are due here. First of all, let us consider the case of a Bose–Bose mixture, i.e., $\Omega \to 0$. In this case, $f(\alpha \to 0) \to 0$ and the spin-dipole susceptibility is simply proportional to the magnetic susceptibility equation (12). Therefore, also $\chi_{\rm sd}$ diverge at the (miscible/immiscible) transition point $g_{ab} \to g$ [5]. Physically, this is due to the fact that the two gases become globally immiscible at the transition point since the

[4] Notice that the domain of the function $f(\alpha)$ (to be real), i.e., $1/\alpha \geqslant -1$, is precisely where the system is fully paramagnetic.

[5] At the same point, but for finite Ω, one has $f(\alpha \to \infty) \to -1 + 2/(5\alpha)$ and therefore $D/d = gn_0/(5\Omega)$.

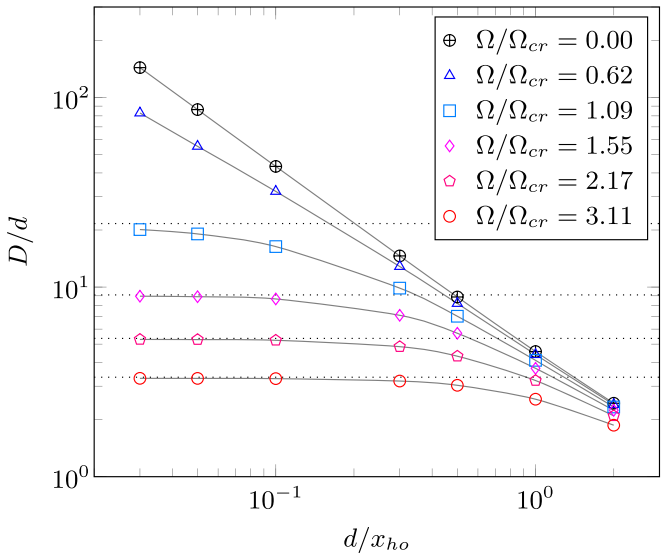

Figure 3. Dipole D as a function of traps displacement d for different values of Ω/Ω_{cr} and for $g_{ab}/g = 1.1$ as in figure 2. Dotted lines are analytical results from equation (15) for the four bigger values of Ω, points are numerical data and grey full lines are only a visual guide.

latter condition is density independent. As we will see in the next section, the divergence of χ_{sd} leads to a zero frequency (soft) spin-dipole mode.

By contrast, for finite Ω the paramagnetic/ferromagnetic transition point, namely $g_{ab} = g + \Omega/n_0$, depends on the density. Therefore, the spinor gas starts becoming ferromagnetic at the centre of the trap only. The quantity χ_{sd}, being density integrated, remains finite at the transition point (indeed $f(-1) = -3$) leading (see next section) to a finite frequency for the spin-dipole mode. This behaviour is very general and it has already been pointed out for the Stoner (or itinerant ferromagnetic) instability in the context of cold gases by two of us [29].

Above the critical point the response of the system is no longer linear. The system is *partially ferromagnetic* and has the tendency to form a magnetic domain wall at the centre of the trap (see appendix).

A detailed analysis of the behaviour of D/d is shown in figure 3 where we calculate numerically the spin-dipole of the gas as a function of the trap separation d with the choice $g_{ab}/g = 1.1$. Above the critical Rabi frequency we see that indeed linear response applies and the analytical expression equation (15) works very well. Notice that the spin-dipole moment allows for a clear identification of the phase transition point, above which the induced dipole moment D changes its behaviour as a function of d.

4. Spin dipole dynamics

In this section we study the dynamics of the system. In particular we prepare the system initially in the ground state of very slightly displaced external potential and then suddenly set the displacement to zero. As one can expect, the physics is completely different depending on whether the system is paramagnetic or ferromagnetic. In the earlier case the system shows a well defined out-of-phase oscillation, the spin-dipole mode. The previously calculated spin-dipole polarizability plays an important role in characterizing the behaviour of the spin-dipole frequency [29, 30]. Notice in particular that for two independent condensates ($\Omega = g_{ab} = 0$) the spin-dipole frequency simply coincides with the trap frequency ω_{ho}. In the ferromagnetic case the system evolves according to a highly non-linear dynamics and it shows ground state selection. We analyze the two cases separately in the next two sections. Some details on the numerical solution of the GP equations can be found in appendix B and reference therein. For the interested reader we include in the supplementary material the real time evolution of the system in different regimes.

4.1. Paramagnetic phase: sum rule approach

In the paramagnetic phase, as shown in figures 2(a4)–(b4), a small trap displacement corresponds to a small deviation with respect to the ground state at zero displacement and therefore linear response theory can be applied. The dynamics we consider in this case coincides with the dynamical response of the spinor gas to the spin-dipole operator $\hat{S}_d = \sum_{i=1}^{N} x_i \hat{\sigma}_{z,i}$. A very powerful tool to estimate the frequency of collective modes is the so-called sum rule approach [31, 32]. This approach has been very successfully employed for the dynamics of

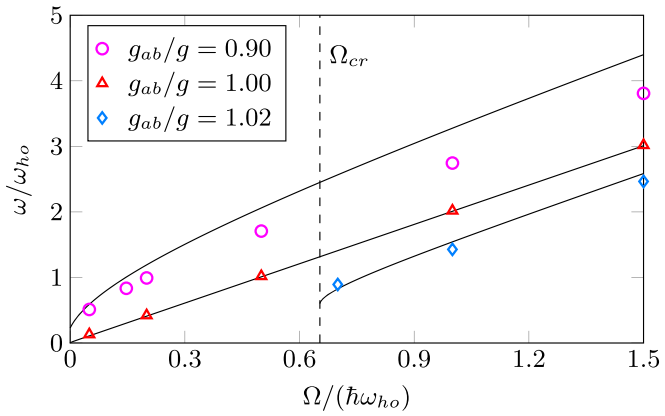

Figure 4. Spin-dipole frequency as a function of Ω for different values of interactions. Lines are analytical results from equation (20) and points are numerical data. In order to have a fully paramagnetic phase for $g_{ab} > g$, one needs $\Omega \geqslant \Omega_{\rm cr}$ (see text and equation (5)), the value of $\Omega_{\rm cr}$ for $g_{ab}/g = 1.02$ (blue diamonds) is shown by the dashed line. In the supplementary material, two videos show the oscillations of the clouds for $g_{ab}/g = 0.9$ and $g_{ab}/g = 1$ (both at $\Omega = 0.5\hbar\omega_{\rm ho}$): 1.0 sec of the video corresponds to $1.0\omega_{\rm ho}t$.

both cold gases and nuclei. We give a simple reminder here that sum rules are defined for an operator $\hat{F}$ as

$$m_k(F) = \sum_n |\langle 0|\ \hat{F}\ |n\rangle|^2 \left(E_n - E_0\right)^k, \tag{16}$$

and they represents the moments of the strength distribution function relative to $\hat{F}$. The sum rule approach has the merit of providing a direct way to obtain an upper bound of collective mode frequency through the ratio of different sum rules, and therefore gives an understanding of the collective mode frequency in terms of static macroscopic quantities [32].

In our case the operator of interest is $\hat{S}_{\rm d}$ and we we use the energy weighted and inverse energy weighted sum rule, i.e.,

$$\hbar^2\omega_{\rm SD}^2 \leqslant \frac{m_1\left(S_{\rm d}\right)}{m_{-1}\left(S_{\rm d}\right)}. \tag{17}$$

They are particularly suitable in our case. The energy weighted one (m_1) is easily rewritten in terms of a double commutator as $m_1 = (1/2)\langle 0|[S_{\rm d}, [H, S_{\rm d}]]|0\rangle$. The only terms in H that do not commute with S_d are the kinetic energy and the Rabi coupling $H_{\rm R} = -\Omega\sum_i \hat{\sigma}_{x,i}$. The former gives the usual $N\hbar^2/(2m)$ contribution, while the latter is straightforwardly evaluated as $-4\Omega x^2\hat{\sigma}_x$. Averaging on the ground state, we obtain the result

$$m_1 = N\frac{\hbar^2}{2m} + 8\Omega\int_0^{R_{\rm TF}} x^2 n_0(x)\,{\rm d}x. \tag{18}$$

The inverse energy weighted sum rule (m_{-1}) is directly related to the susceptibility of the ground state through the relation

$$m_{-1} = \frac{N}{2}\chi_{\rm sd}, \tag{19}$$

and using the definition equation (10) together with the result equation (14) we obtain the following upper bound to the spin-dipole frequency

$$\omega_{\rm SD}^2 = {\omega_{\rm ho}}^2\left(\frac{g - g_{ab}}{g + g_{ab}}\right)\left[\frac{1 + 8\Omega n_0\left(g + g_{ab}\right)/\left(5\hbar\omega_0^2\right)}{1 + f\left(\Omega/\left(\left(g - g_{ab}\right)n_0\right)\right)}\right]. \tag{20}$$

Notice that the equality in equation (17) is attained when the whole strength is exhausted by a single state.

In figure 4 the sum-rule result is compared with the predictions of the solutions of a time dependent Gross–Pitaevskii calculation. As already mentioned from the numerical or experimental point of view, the excitation of the spin-dipole mode is achieved starting with an equilibrium configuration in the presence of slightly displaced trapping potentials, as described by equation (8), and suddenly setting $d = 0$.

Notice that at the transition point the frequency does not go to zero, since for the reasons explained in the previous section $\chi_{\rm sd}$ (or m_{-1}) does not diverge at that point. This has to be compared with the mixture case, which is recovered sending $\Omega \to 0$. In this case the spin-dipole frequency vanishes close to the critical point following the law

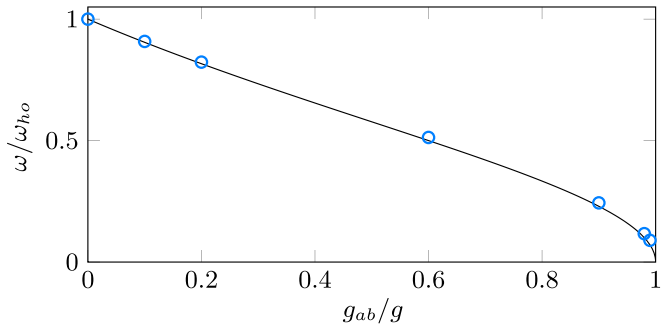

Figure 5. Spin-dipole frequency for a Bose–Bose mixture, i.e. $\Omega = 0$, as a function of the ratio g_{ab}/g. Line is the analytical result and points are numerical data. In this case the spin-dipole frequency goes to zero at the phase separation transition point.

$$\omega_{\mathrm{SD}}(\Omega = 0) = \omega_{\mathrm{ho}}\sqrt{\frac{g - g_{ab}}{g + g_{ab}}}, \tag{21}$$

and the sum-rule approach gives the exact result as shown in figure 5.

Sum-rules give the exact result also for the intrinsic $SU(2)$ symmetric point $g_{ab} = g$ (and $\Omega \neq 0$ in general) and $g_{ab} = g$ as it can be seen in figure 4) (red triangles). The magnetic energy of the spinor gas in this regime depends on the relative density only through the Rabi coupling, which breaks the $SU(2)$ symmetry of the system. The spin-dipole frequency behaves in this case as

$$\omega_{\mathrm{SD}}\left(g_{ab} = g\right) = 2\Omega\sqrt{1 + \frac{5}{16}\frac{\hbar\omega_{\mathrm{ho}}^2}{g n_0 \Omega}} \tag{22}$$

which is essentially twice the Rabi frequency and therefore almost independent of the tapping frequency. The latter unusual result for a trapped gas is due to the correlation between the internal and external degrees of freedom that in particular lead to the modification of the f-sum rule, see equation (18).

In the more general case, when both Ω and $(g_{ab} - g)$ are different from zero, the frequency is given by the full equation (20) in which both the coherent and the interspecies s-wave couplings play a role. In this more general case one observes that the sum rule approach provides only an upper bound to the numerical solution, due to the appearance of more frequencies in the numerical signal resulting in beating effects.

In the supplementary material we include two videos showing the oscillations of the clouds in the paramagnetic case for $g_{ab}/g = 0.9$ and $g_{ab}/g = 1$ and $\Omega = 0.5\hbar\omega_{\mathrm{ho}}$. The real time evolution shows clearly the presence of only one frequency in the intrinsic $SU(2)$ symmetric case and the appearance of more frequencies when $g_{ab} \neq g$.

4.2. Ferromagnetic phase: ground state relaxation

In the previous section we studied the dynamics for a completely paramagnetic gas, i.e., $\Omega > \Omega_{\mathrm{cr}}$. The behaviour is very different when the system presents a ferromagnetic behaviour. In this case the ground state of the system with equal trapping potentials is polarized as shown in figure 2 plots (a2) and (a3). When the traps are shifted, the ground state is instead globally unpolarized ($N_a = N_b$) but with a large spin-dipole moment (depending on the values of Ω and d) as one can see in figure 2, plots (b2) and (b3). Therefore, the initial state and the ground state are very far from each other. This circumstance results in a non-trivial non-linear dynamics as shown by the dynamics of the spin-dipole and of the polarization reported in figure 6. At the beginning, the spinor gas oscillates around the initial configuration, trapped in the unpolarized state. After a certain time, τ_{wait}, the domain wall starts moving and a finite polarization appears. The system then bounces back and forth between the initial magnetic state and its magnetic ground state to eventually relax to the latter one[6]. An example of such dynamics can be viewed in the video in the supplementary material. If the global polarization of the ground state is large, the effects of non-linearity and the number of bounces are large. When the system is slightly in the ferromagnetic regime, no bounces are observed and the system after τ_{wait} soon reaches its ground state (see right lower panel in figure 6). Notice that even if the system is isolated, it can approach in the long time limit an asymptotic steady state, as a result of destructive interference of several time oscillating factors, present in the evolution of expectation values of observables. Specifically, in the case of a large and dense collection of

[6] The system is closed and energy conserving and still able, in the long time limit, to approach and select one of the two possible ground states. The final state obviously presents still (small) oscillations around its ground state.

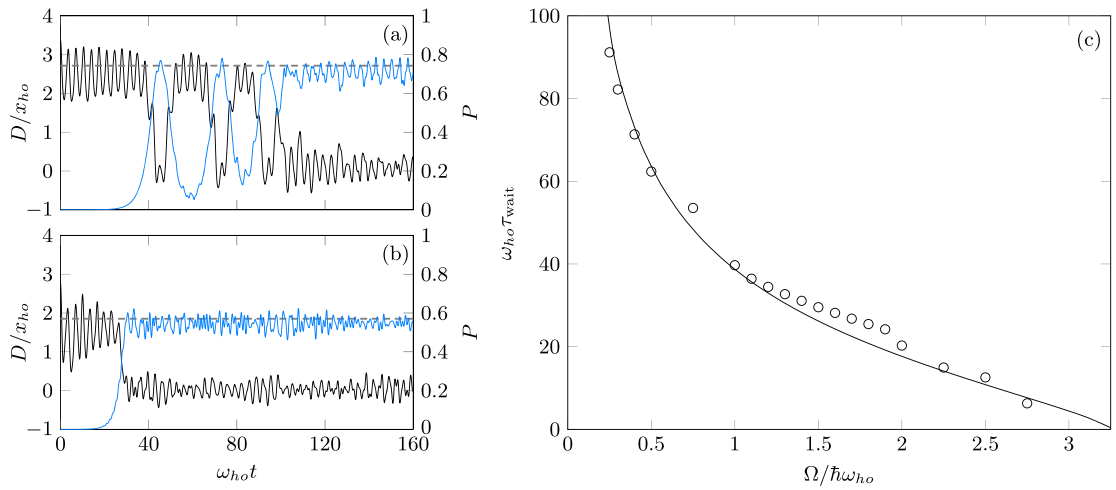

Figure 6. (a) and (b): real time spin-dipole oscillation (black solid lines), polarization of the system (blue solid lines) and ground state polarization values (dashed lines); parameters are $g_{ab} = 1.1g$, $g/(\hbar\omega_{\rm ho}x_{\rm ho}) = 5$ and $\Omega/\hbar\omega_{\rm ho} = 1.5$ (a), $\Omega/\hbar\omega_{\rm ho} = 2$ (b). In the supplementary material a video shows the oscillation of the clouds of panel (a), 1.0 sec of the video corresponds to $1.0\omega_{\rm ho}t$. (c): waiting time as a function of Ω; points are numerical data and line is a fit of data with function $A\sqrt{\sigma}$ where σ is the surface tension of equation (23).

frequencies, the interference phenomenon results in a dephasing mechanism similar to inhomogeneous dephasing.

The total energy of the system is still conserved, the algorithm used (see appendix B) does not contains any dissipative mechanism and we explicitly check that the total energy does not change during the evolution. At the end of the real time evolution we get the ground state profile superposed with some high frequency perturbations carrying the extra energy.

As we have already mentioned in section 2, the initial configuration in the ferromagnetic case contains a domain wall at the centre of the trap. We have identified a close relation between the observed waiting time and the square root of the domain wall energy (see appendix A)

$$\sigma \propto \frac{\left|\left(g - g_{ab}\right)n \;+\; 2\Omega\right|^{3/2}}{\Omega}. \tag{23}$$

From an intuitive point of view, the higher is the energy of the domain wall, σ, the more time is required for the system to relax from the kink into one of the ground states of the system; accordingly, there is expected to be a relation of proportionality between the waiting time and σ. A standard field theoretical estimate of the average tunnelling time cannot be straightforwardly performed since only close to the transition does our field theory resemble an ordinary ϕ^4 theory (see appendix A for details); for this reason, we took advantage of a numerical fit to extract with surprising accuracy the relation, $\tau_{\rm wait} \propto \sqrt{\sigma}$, as shown in figure 6.

The fact that for $\Omega \to 0$ the waiting time diverges can be easily understood noticing that the initial state and the ground state are very far from each other (see, e.g., panels (a2) and (b2) of figure 2). Eventually, in the strict $\Omega = 0$ case, the system cannot reach the totally polarized ground state and it remains in the phase separated state (see panels (a1) and (b1) of figure 2).

5. Conclusions

In the present work we analyze in details the static and dynamic response of a trapped coherently driven two-component condensate to spin-dipole probe. We show that the spin-dipole susceptibility is a good quantity able to identify the appearance of a ferromagnetic-like region in the cloud.

For the dynamics we study the spin-dipole mode frequency by starting in a configuration with displaced harmonic potentials, which are suddenly brought to the same value. When the system is paramagnetic, such a frequency is well reproduced by a sum-rule approach. In particular the *f*-sum rule is strongly modified by the Rabi coupling in the symmetric interaction case ($(g = g_{ab})$ and the inverse energy sum rule is proportional to the spin-dipole susceptibility and coincides with the second spatial momentum of the local magnetic susceptibility (see equation (14)).

When the system has a ferromagnetic domain, a linear response cannot be applied anymore and the dynamics is highly non-linear. The initial configuration within displayed potentials is unpolarized and contains

a magnetic kink centred at the origin. The dynamics is trapped for a time, $\tau_{\rm wait}$, in the initial configuration, after which the system is able to relax to its polarized ground state. We find that $\tau_{\rm wait}$ is proportional to the square root of the kink surface tension.

Our study improves the characterization of coherently driven BECs, enlightening their differences with respect to Bose–Bose mixtures. Moreover, measuring the spin-dipole dynamics opens new perspective to experimentally access important magnetic properties of the system, e.g., its susceptibility or the domain wall surface tension.

Acknowledgments

AR acknowledges useful discussions with Marta Abad, Markus Heyl, Nicolas Pavloff and Wilhelm Zwerger, and support from the Alexander von Humboldt foundation. A.S. acknowledges Komet 337 group of their Johannes Gutenberg Universität Mainz for their kind hospitality. This work has been supported by ERC through the QGBE grant and by Provincia Autonoma di Trento.

Appendix A. Magnetic domain wall surface tension

In this appendix we briefly show how to approximate the energy functional for the magnetization for a spinor condensate with a classical one-dimensional ϕ^4 (Ginzburg–Landau for the phase transition) theory [33]. From the latter it is easier to show the existence of a kink or domain wall in the magnetization, and we compute in this regime its surface tension. In the symmetric case $g_a = g_b = g$ and considering a uniform total density $n = n_a + n_b$, the relative density or magnetization $M = (n_a - n_b)/n$, enters in the energy density

$$E(M) = \int dx \left[\frac{\hbar^2 n (\nabla M)^2}{8m\left(1 - M^2\right)} + W(M) \right], \tag{A.1}$$

where the first term arises from the kinetic energy and the term

$$W(M) = \frac{n^2}{4}\left(g - g_{ab}\right)M^2 - \Omega n\sqrt{1 - M^2}, \tag{A.2}$$

accounts for the density–density interaction and the Rabi terms For a homogeneous magnetization, minimisation $\delta E/\delta M = 0$ leads to the usual equation for the paramagnetic- and ferromagnetic-like states. From equation (A.1) one sees that close to the phase transition, i.e., $M \ll 1$ a standard Ginzburg–Landau theory for the order parameter M, is valid, where the kinetic energy is just the square of the gradient of M and the effective potential takes the usual quadratic plus quartic form

$$\begin{aligned} W(M) &= \frac{n^2}{4}\left(g - g_{ab} + \frac{2\Omega}{n}\right)M^2 + \frac{n\Omega}{8}M^4 \\ &\equiv \frac{r}{2}M^2 + \frac{u}{4}M^4. \end{aligned} \tag{A.3}$$

As usual, the $\mathbb{Z}_2$ symmetry broken ground state is obtained for $r < 0$. A kink in M is the field solution interpolating between the two degenerate minima. Its surface tension, σ, which coincides with its energy in a one-dimensional situation, can be easily computed [34] yielding the result

$$\sigma \propto \sqrt{\frac{\hbar^2 n^2}{m}\frac{|r|^{3/2}}{u}} \propto \sqrt{\frac{\hbar^2 n^2}{m}\frac{|\delta g n + 2\Omega|^{3/2}}{\Omega}} \tag{A.4}$$

Appendix B. Numerical method

All numerical data presented in this paper have been obtained solving the GP coupled equations by means of the split-operator method and by treating the kinetic term in Fourier space [35, 36]. The initial wave functions $\psi_a(x, t)$ and $\psi_b(x, t)$ are evolved for a time step Δt alternately by the kinetic, potential and Rabi terms of Hamiltonians in equation (1):

$$\begin{aligned} \tilde{\psi}_i(k, t) &\mapsto \mathrm{e}^{-ik^2\Delta t/2}\tilde{\psi}_i(k, t) \\ \psi_i(x, t) &\mapsto \mathrm{e}^{-i\left(V_i + g|\psi_i|^2 + g_{ab}|\psi_j|^2\right)\Delta t}\psi_i(x, t) \\ \psi_i(x, t) &\mapsto \cosh(-\Omega\Delta t)\psi_i(x, t) + \sinh(-\Omega\Delta t)\psi_j(x, t) \end{aligned} \tag{B.1}$$

where $i = a,\ b \neq j$ and equation (B.1) is for the imaginary time evolution. One can simply obtain the same set of equations for real time evolution by changing Δt in $i\Delta t$.

An algorithm of this typ is symplectic; this means that the method exactly simulates a Hamiltonian $H_{\Delta t}$ with $H_{\Delta t} - H$ a power series in Δt. The advantages of using symplectic integrators are that there is no drift in energy due to the exact conservation of $H_{\Delta t}$ and the phase-space volume is exactly conserved.

In order to obtain the ground states we ran the imaginary time evolution starting from an initial trial wave function built from both random density and phase distributions, in order to prevent the algorithm from reaching false metastable states. For the dynamics we loaded the ground states obtained with displaced traps and let them evolve using the same algorithm but with real time and with the equal trapping potential Hamiltonian. The values of polarization P and of spin-dipole moment D are calculated and saved at each time step and then analyzed to obtain the frequencies. This last step is not always so straightforward—sometimes the signal contains more than one frequency and damping occurs. In such cases we perform a Fourier analysis of the data and we keep the maximum-amplitude frequency.

References

[1] Andreev A F and Bashkin E P 1975 *Sov. J. Exp. Theor. Phys.* **42** 164
[2] Shevchenko S I and Fil D V 2007 *JETP* **105** 135
[3] Beattie S, Moulder S, Fletcher R J and Hadzibabic Z 2013 *Phys. Rev. Lett.* **110** 025301
[4] Chang M-S, Qin Q, Zang W L, You L and Chapman M S 2005 *Nat. Phys.* **1** 111
[5] Zibold T, Nicklas E, Gross C and Oberthaler M K 2010 *Phys. Rev. Lett.* **105** 204101
[6] Cirac J I, Lewenstein M, Mo K and Zoller P 1998 *Phys. Rev.* A **57** 1208
[7] Gross C, Strobel H, Nicklas E, Zibold T, Bar-Gill N, Kurizki G and Oberthaler M K 2011 *Nature* **480** 219
[8] Son D T and Stephanov M A 2002 *Phys. Rev.* A **65** 063621
[9] Kasamatsu K, Tsubota M and Ueda M 2004 *Phys. Rev. Lett.* **93** 250406
[10] Deconinck B, Kevrekidis P G, Nistazakis H E and Frantzeskakis D J 2004 *Phys. Rev.* A **70** 063605
[11] Lee C, Hai W, Shi L and Gao K 2004 *Phys. Rev.* A **69** 033611
[12] Sabbatini J, Zurek W H and Davis M J 2011 *Phys. Rev. Lett.* **107** 230402
[13] Bernier N R, Dalla Torre E G and Demler E 2014 *Phys. Rev. Lett.* **113** 065303
[14] Dalibard J, Gerbier F, Juzeliūnas G and Öhberg P 2011 *Mod. Phys. Rev.* **83** 1523
[15] Blakie P B, Ballagh R J and Gardiner C W 1999 *J. Opt. B: Quantum Semiclass. Opt.* **1** 378
[16] Nicklas E, Strobel H, Zibold T, Gross C, Malomed B A, Kevrekidis P G and Oberthaler M K 2011 *Phys. Rev. Lett.* **107** 193001
[17] Goldstein E V and Meystre P 1997 *Phys. Rev.* A **55** 2935
[18] Tommasini P, Passos E J V D, Piza A F R D T and Hussein MS 2003 *Phys. Rev.* A **67** 023606
[19] Matthews M R, Anderson B P, Haljan P C, Hall D S, Holland M J, Williams J E, Wieman C E and Cornell E A 1999 *Phys. Rev. Lett.* **83** 3358
[20] Williams J, Walser R, Cooper J, Cornell E A and Holland M 2000 *Phys. Rev.* A **61** 033612
[21] Shelykh I, Kavokin A, Rubo Y, Liew T and Malpuech G 2007 *Superlattices Microstruct.* **41** 313
[22] Shelykh I, Kavokin A, Rubo Y, Liew T and Malpuech G 2010 *Semicond. Sci. Technol.* **25** 103001
[23] Silaev M and Babaev E 2012 *Phys. Rev.* B **85** 134514
[24] Pitaevskii L P and Stringari S 2003 *Bose-Einstein Condensation* (Oxford: Oxford University Press)
[25] Abad M and Recati A 2013 *Eur. Phys. J.* D **67** 148
[26] Ho T-L and Shenoy V B 1996 *Phys. Rev. Lett.* **77** 3276
[27] Svidzinsky A A and Chui S T 2003 *Phys. Rev.* A **68** 013612
[28] Riboli F and Modugno M 2002 *Phys. Rev.* A **65** 063614
[29] Recati A and Stringari S 2011 *Phys. Rev. Lett.* **106** 080402
[30] Li Y, Martone G I and Stringari S 2012 *Europhys. Lett.* **99** 56008
[31] Bohigas O, Lane A and Martorell J 1979 *Phys. Rep.* **51** 267
[32] Lipparini E and Stringari S 1989 *Phys. Rep.* **175** 103
[33] Landau L D and Lifshitz E M 1980 *Statistical Physics Part1* (Oxford: Pergamon)
[34] Weinberg E 2015 *Classical Solutions in Quantum Field Theory: Solitons and Instantons in High Energy Physics* (Cambridge: Cambridge University Press)
[35] Bao W, Jin S and Markowich P A 2003 *SIAM J. Sci. Comput.* **25** 27
[36] Bao W, Jaksch D and Markowich P A 2003 *J. Comput. Phys.* **187** 318